Extreme-ultraviolet high-order harmonic generation from few-cycle annular beams

Originally published in:
Optics Letters 43(18), https://doi.org/10.1364/OL.43.004506

Extreme-ultraviolet high-order harmonic generation from few-cycle annular beams

THOMAS GAUMNITZ[1*], AROHI JAIN[1], AND HANS JAKOB WÖRNER[1]

[1] Laboratorium für Physikalische Chemie, ETH Zürich, Vladimir-Prelog-Weg 2, 8093 Zürich, Switzerland
[*] Corresponding author: Thomas.Gaumnitz@phys.chem.ethz.ch

Compiled August 2, 2018

An annular infrared (IR) laser beam has been used for high-order harmonic generation reaching a cut-off energy of 90 eV for XUV-IR pump-probe experiments in an intrinsically stable attosecond beamline. The generation of harmonics along the laser axis in the missing portion of the laser beam decreases the IR power load on thin metallic foils that are used for removing the residual IR and shaping the extreme ultraviolet pulses from the HHG. This finds applications in high average power few-cycle laser systems, where high average IR power destroys the foils. The spatial separation of IR and XUV will moreover simplify the realization of attosecond time-resolved measurements.

OCIS codes: (320.7100) Ultrafast measurements; (140.7240) UV, EUV, and X-ray lasers; (320.6629) Supercontinuum generation.

http://dx.doi.org/10.1364/ao.XX.XXXXXX

1. INTRODUCTION

With the discovery of high-harmonic generation (HHG) [1, 2] a new field of physics was born. This field called attosecond science [3] is used to study atoms [4] and molecules on their shortest timescales, to understand electronic processes like charge migration [5], bond breaking [6, 7] and formation and photoionization dynamics [8]. Attosecond science and attosecond spectroscopy have driven laser and source development to reach higher cut-off energies and higher photon fluxes. The typical work horse in most laser laboratories are Titanium:Sapphire laser systems [9, 10] that deliver a few millijoule pulse energy at kilohertz repetition rates with pulse durations down to the few-cycle regime at around 0.8 μm. By focusing the laser beam into a gaseous medium [11] at typical intensities of about $I \approx 10^{14}\,\mathrm{Wcm}^{-2}$, high-order harmonic radiation with photon energies up to 100-150 eV (photon energies up to 1.3 keV have been observed [12], 1.7 keV using longer-wavelength drivers [13], with new records in pulse duration of 43 as [14]) at a few nanojoules pulse energy (conversion efficiency 10^{-6} [15]) can be generated that co-propagates with the fundamental laser. During the last decade, attosecond XUV-IR pump-probe experiments using HHG from (few-cycle) femtosecond laser pulses have become a very standard technique. The relatively low pulse energy requires short focal lengths to achieve the necessary intensities ($(0.1-1)\cdot 10^{15}\,\mathrm{Wcm}^{-2}$) for the high harmonic generation process. For many time-resolved pump-probe experiments, the residual laser light has to be suppressed to avoid the ionization of the target material. Suitable methods are spatial separation or spectral filtering. Spatial separation of the intense fundamental laser beam can be achieved using a grating in the beam. This approach is typically used in monochromator setups [16]. Another possibility to suppress the residual IR radiation for low average laser power is filtering by thin metallic foils, that are transparent to the XUV radiation [9, 10, 17], or using a micro-channel plate detector [18]. With the recent development in laser sources, high power, high-repetition laser sources are now available from OPCPA [19, 20] or fiber [21, 22] lasers. These system are capable to deliver pulse energies of several 100 μJ at several 10-100 kHz repetition rate. Due to high laser intensity, especially in the center of the beam, in conjunction with high average power (e.g. 1 mJ @100 kHz = 100 W average power) apertures, slits, filters and the grating surface are prone to damage or degradation. The application of these new laser sources to attosecond time-resolved measurements calls for the development of new experimental techniques that can handle the associated high average powers. To mitigate this, high-order harmonic generation can be performed with an annular laser beam, such that the center part of the beam is cut away. This has been experimentally realized by either inserting a laser block which reduces the total energy by half [23] or using a phase mask [24] to block the IR in the center and to allow for RABBITT measurements. However, for those experiments, EUV photon energies up to 16 eV [24] only were reached. These techniques can not be used for high average power as the thermal load is too high. Annular beams, prepared with an annular pupil filter, have also shown to improve spatial resolution in the focal plane, demonstrating applications in two photon microscopy [25]. Another approach, that introduce minimum energy losses to the beam, is the usage of an axicon [26].

In this manuscript, we present high-order harmonic generation in the XUV region with a few-cycle laser pulse using an annular beam with the cut-off reaching up to E_{cut} = 90 eV and compare it with HHG using a full Gaussian beam. The perforated mirror used to create an annular beam, can sustain high intensity/power levels. In the focus, the beam intensity has a Bessel profile, whereas in the far-field, the hole is reproduced.

This allows the usage of metallic foils for spectral filtering between XUV and IR beam and enables collinear pump-probe experiments with high-power high-repetition-rate laser systems. We discuss the beam intensity distribution in the focal plane using the scalar diffraction theory [27], and SFA calculations including propagation to simulate HHG spectra, which we compare to our experimental results.

2. BEAM INTENSITY DISTRIBUTION

To calculate the intensity distribution of a Gaussian annular beam in the focus and the far-field, we consider a Gaussian optical beam of wavelength λ, and with beam diameter $D = 2a$, with an area $A = \pi a^2$. The beam is incident on a perforated/annular mirror with hole diameter $\epsilon D = 2\epsilon a$ which generates an annular beam with the obscuration factor $0 \leq \epsilon < 1$. The perforated mirror (or aperture) is assumed to be located at $z = 0$, where z is the propagation direction of the beam (cf. Fig. 1). For a Gaussian beam profile, the intensity distribution $I_g(\rho)$ at the annular mirror [27] can be written as:

$$\begin{aligned} I_g(\rho) &= (P_0/A) f(\gamma,\epsilon) \exp(-2\gamma\rho^2), \text{where} \\ f(\gamma,\epsilon) &= 2\gamma / \left[\exp(-2\gamma\epsilon^2) - \exp(-2\gamma)\right] \end{aligned} \quad (1)$$

where ρ is described in units of a, with $\epsilon \leq \rho \leq 1$. Here, $\epsilon = 0$ corresponds to the beam reflected from the full mirror. $\sqrt{\gamma}$ represents the ratio of mirror diameter to the beam diameter, and is set to $\sqrt{\gamma} = 1$ for the following discussion. Irrespective of the size of the hole, a fixed total power P_0 is transmitted through the aperture. This is to exclude the effect of intensity variation due to power loss and exclusively explore the effect of the annular beam. At the annular mirror, the intensity levels for the Gaussian annular beam are higher compared to a Gaussian beam, as both correspond to same power, however distributed over a smaller area. The beam is then focused at a distance f from the annular mirror. The intensity distribution in the focal plane along the radial direction of the beam can then be obtained using the scalar diffraction theory [27]:

$$I_g(r,f) = 4 \cdot f(\gamma,\epsilon) \left[\int_\epsilon^1 \exp(-2\gamma\rho^2) J_0(\pi r\rho)\rho \mathrm{d}\rho\right]^2 \quad (2)$$

and along the direction of propagation z at $r = 0$ corresponds to:

$$I_g(0,z) = \left[\frac{f}{z}\right]^2 \frac{2\gamma}{(A/\lambda(1/z - 1/f))^2 + \gamma^2} \times \left\{\coth\left[(1-\epsilon^2)\gamma\right] - \frac{\cos\left[(1-\epsilon^2)\left(A/\lambda(1/z - 1/f)\right)\right]}{\sinh\left[(1-\epsilon^2)\gamma\right]}\right\} \quad (3)$$

Here J_0 is the zero order Bessel function, and r is in units of $\lambda z/D$. The intensity distribution $I_g(r,z)$ is in units of $P_0 A/\lambda^2 R^2$. Fig. 1 shows a schematic representation of a focusing annular beam.

Fig. 1b shows the intensity distribution in the focal plane along the radial direction. The annular Gaussian beam focuses to a Bessel like beam in the radial direction. We set a wavelength of $\lambda = 800$ nm and choose ϵ=0, 0.33 and 0.66. The focal length is set to $f = 500$ mm and the initial beam diameter ($1/e^2$ width) is chosen to be $D = 9$ mm. The hole in the beam, leads to reduction in intensity and the beam diameter at the focus or the point of high harmonic generation, evident for increasing values of ϵ. It also results in the generation of side lobes in the radial spatial profile, where the energy from the central peak is transferred.

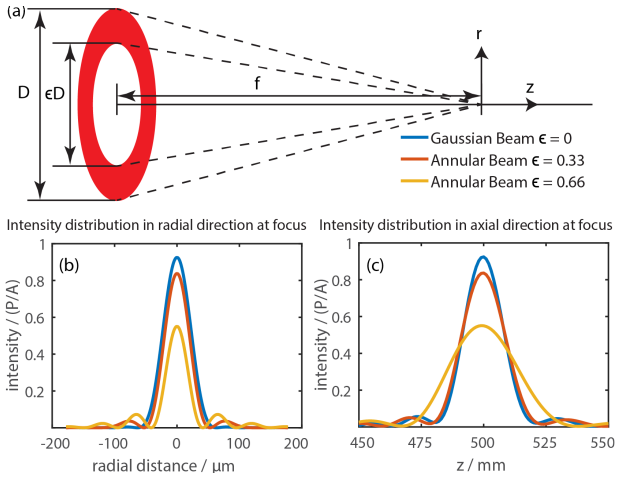

Fig. 1. Schematic representation of a focusing annular beam. (a) Annular beam geometry for an NIR pulse with inner diameter ϵD and outer diameter D, being focused at distance f. Intensity distribution at the focusing point along the radial direction (b) and along the axial direction (c) for a Gaussian and annular beam of different ϵ.

Depending on the size of the hole, the ratio of central peak intensity I_0 to the side lobe (secondary maxima) is less than $0.1 \cdot I_0$, it is safe to assume that no HHG in the region of the side lobe, as the cut-off energy scales as $E_{\text{cut}} \propto 3.17 U_p \propto 3.17 I\lambda^2$. The calculated beam intensity distribution along the propagation axis is shown in Fig. 1c. The far field profile of the IR beam intensity distribution starts to correspond to the distribution at the annular mirror, also shown in Fig. 2c. However, the center of the beam now contains the generated harmonics. The region of high intensity of IR is well separated from the region of XUV radiation. This property has been utilized to prevent degradation of the metallic foils and multilayer mirrors.

3. EXPERIMENTAL SETUP

In Fig. 2a a schematic of our setup is shown, where we have used a 1 kHz Ti:Sapphire laser centered at $\lambda = 800$ nm (Femtolasers Rainbow 4 with feed-forward CEP stabilization, Femtopower V pro, $E = 5.5$ mJ) for HHG. The amplifier output is compressed to a pulse duration of $\tau = 23$ fs ($\tau_{\text{FTL}} = 19$ fs) with a transmission grating compressor. A small fraction of the pulse energy is directed to an f-2f-interferometer for CEP stabilization of the amplifier, where about $E_{\text{fiber}} = 1.6$ mJ are focused ($f_{\text{fiber}} = 1.25$ m) into a static filled ($p_{\text{fiber}} = 1.6$ bar neon) rigid hollow core fiber ($\varnothing = 250\,\mu$m) to broaden the spectrum, where a beam pointing stability system (TEM Aligna) is used to compensate for beam drifts. After re-collimation behind the fiber, the pulses are compressed using chirped mirrors (UltraFast Innovations, PC70, double angle technology) to a pulse duration of $\tau \approx 5.5$ fs ($\tau_{\text{FTL}} \approx 3$ fs) at a pulse energy of approximately 700 μJ. A pair of wedges under Brewster's angle is used for fine adjustment of the pulse duration and allows for best compression conditions for the high-harmonic generation process and the highest flux of the generated high-order harmonics. A wave plate can be introduced in the IR beam path for angular resolved photoelectron measurements using our intrinsically stable attosecond beamline [28] that comprises a time-of-flight spectrometer [29].
The full Gaussian beam ($F^{\#} \approx 56$) with a pulse energy of about 280 μJ is focused onto a neon gas target ($p \approx 100 - 200$ mbar)

for high-harmonic generation. The generation target is a differentially pumped finite target and the HHG spectrum obtained using the full Gaussian beam, is shown in Fig. 3. We then use a perforated flat silver mirror with a $d = 3$ mm hole in the center as shown in Fig. 2b, at 0° angle of incidence, to prepare the annular beam. It is placed before the focusing mirror Fig. 2a, resulting in a doughnut shaped beam. The diameter of the hole was chosen such that the heat load is minimized on the thin metallic filter (⌀ 2.8 mm) matching with the imaging conditions. A beam dump behind the perforated mirror blocks the residual beam. It can also be replaced with re-routing optics to introduce the residual beam in the vacuum chambers for pump-probe experiments. The beam is aligned on the perforated mirror using two steering mirrors as shown in figure 2a, and is then focused into the high harmonic gas cell. A pick-up mirror after the high harmonic generation is used to monitoring the beam after the high harmonic generation. An iris is used to control the IR intensity and the metallic foil shown in Fig. 2c acts as a bandpass filter removing the residual IR and the unwanted XUV radiation. The beam further propagates to the photon spectrometer where the XUV photon spectrum is recorded.

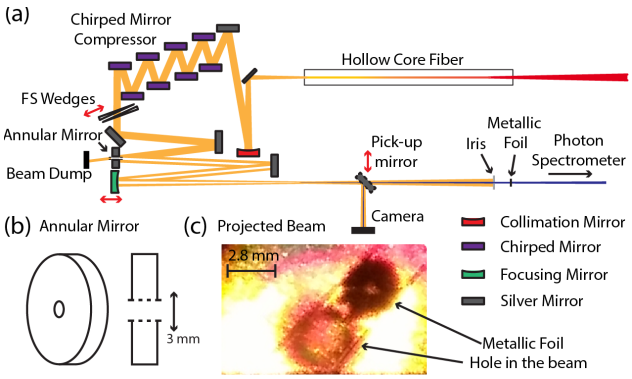

Fig. 2. Schematic of the few-cycle pulse generation and the annular beam preparation. (a) Schematic of the experimental setup, described in Sec. 3 and (b) a perforated mirror with a central hole of 3 mm ($\epsilon = 0.33$). (c) The projected annular beam profile 600 mm after the focus, immediately after the metallic foil taken with a photo-camera. The central hole corresponds to far-field projection of the hole in the mirror and contains the harmonics. By overlapping the metal foil with the hole in the beam, the generated XUV can be filtered and compressed.

4. HHG SPECTRA

Fig. 3 shows the harmonic spectra obtained with our slit-grating HHG spectrometer with the full and the annular beam. For the full beam, a power of 280 mW has been measured in front of the HHG target corresponding with the estimated focus size of $d_f = 110\,\mu$m to a peak intensity of peak intensity of $I = 5 \cdot 10^{14}\,\mathrm{Wcm}^{-2}$. The pressure inside the neon target ($d = 2.5$ mm) has been measured to be $p \approx 120$ mbar in the case of the full beam. For the annular beam, the gas pressure has been increased for optimal generation conditions, while the laser power was reduced to 140 mW, due to the central hole in the beam, leading to half of the peak intensity of the full beam when assuming the same focus spot size. The spectra have been calibrated using the absorption edges of thin metallic filters shown in Fig. 3. Here, a combination of aluminum (red dash-dotted) and zirconium (red) has been used. The HHG spectrum recorded with the full beam is shown as thin blue line. The pulse duration of the input pulse has been determined to be $\tau = 5.5$ fs. The few-cycle nature of our input pulse can be observed in the continuum covering a bandwidth of almost 20 eV, supporting XUV pulse durations of less than 100 as. For the here presented HHG spectrum of the annular beam the CEP has shifted, as the spectrum is fully modulated up to the cut-off. In Fig. 4 the spatial distribution

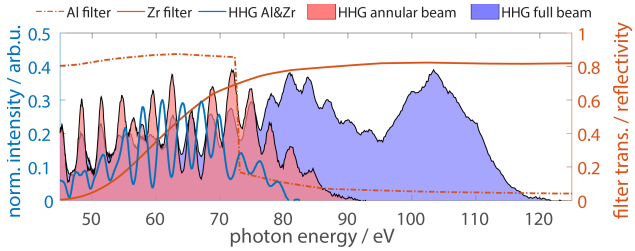

Fig. 3. Experimental HHG spectra recorded with full and annular beam. Normalized HHG spectra recorded with a full (blue) and annular (red) few-cycle pulse together with the filter transmission curves (orange Al (dash dotted) and Zr). HHG recorded with a combined zirconium aluminum filter for calibration (solid blue line). The full beam shows the few-cycle nature by exhibiting a continuum reaching from 95 to 115 eV. During optimization of the annular beam the CEP has been shifted and a strongly modulated cut-off is observed already at 90 eV, as the pulse energy has decreased.

of our HHG spectrum generated by the annular (c) and full (d) beam is presented. For both cases the divergence of the beam decreases with photon energy and the cut-off is pronounced due to the few-cycle pulses used during generation.

The numerical results presented in panel (a) and (b) have been obtained using an adapted version of the HHG simulation code RHYNO [30], where the wave propagation is calculated assuming a cylindrical symmetry for the transverse laser beam profile. The HHG source term is calculated in within the strong-field approximation (SFA) [31]. Ionization is described using the ADK tunneling model [32]. The annular beam calculation has been added to the code. Phase contributions due to free electrons in the generated plasma and the neutral background gas are included during propagation. The simulations were carried out using the measured experiment parameters. A neon target with a length of 2.5 mm with constant pressure (120 mbar) has been assumed, while the pulse duration and the peak intensity were varied. Panel (a) and (b) show the best matching between experiment and theory in terms of cut-off energy, continuum, HHG line structure and HHG yield distribution. For the annular beam, the CEP has shifted during the experiment, thus a sine- instead of a cosine-like pulse is used for the calculations. The agreement between simulation and experiment was found slightly better for an input pulse duration of 6 fs that is slightly longer compared to the measured pulse duration. The peak intensities for the simulations are $7 \cdot 10^{14}\,\mathrm{Wcm}^{-2}$ and $5 \cdot 10^{14}\,\mathrm{Wcm}^{-2}$ for full and annular beam, respectively.

5. DISCUSSION

With our experiment, we have demonstrated that the annular few-cycle beam can be used to generate high-order harmonics, with great potential for applications in the upcoming generation of high-power laser systems [21, 22]. These laser systems with high peak intensities, high power and high repetition rate are

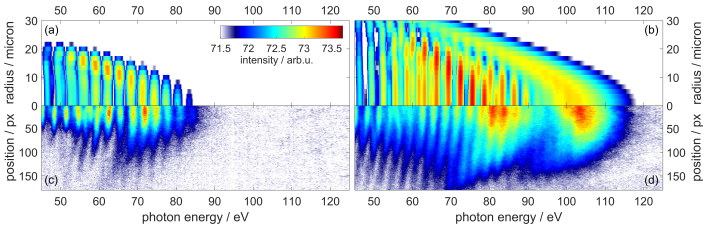

Fig. 4. Measured and simulated HHG spectra for the full and the annular beam. Spatial resolved HHG spectra for the annular beam generated from a mirror with central hole, (panel a, c) and the full beam in panel (b, d). The experimental data is presented in the lower panels. Due to the reduced pulse energy in the annular beam case the cut-off has been reduced from 120 eV to 90 eV and the interaction volume has been decreased by a factor of three due to the tighter focus, as discussed above. The few-cycle nature of the IR pulse is clearly visible in panel (b) and (d) in form of a continuum around the cut-off.

efficient HHG sources. Several experiments recycle the HHG generating IR pulse for pump-probe experiments, e.g., attosecond streaking in the collinear geometry. Metallic foils used to filter the IR beam are a few hundred nanometer thick, and have only shown to withstand low IR intensities. The annular beam scheme allows to have little or no IR intensity on the metallic foil in a compact setup, without the requirement to extend the beamlines for bigger beam size of IR and hence lower intensity.

The annular mirror used in the experiment serves to separate the XUV radiation and the IR, without damaging the filter. It further increases the lateral resolution. However, the light intensity decreases leading to lower order harmonics. This can be compensated by making the beam size at the annular mirror bigger and having smaller focus, however keeping the hole size constant to allow separation of harmonics. We have further demonstrated that since the annular beam leads to a smaller beam diameter at the focus, and therefore corresponds to a larger lateral spread in the far-field that reduces the heat load on the filter even further.

The residual intense central IR laser that leaks out from the hole of the mirror can be re-routed, e.g. to perform strong-field ionization measurements or other pump-probe measurements. The residual IR from the HHG process can also be used to align the target molecules [33]. Introduction of a BBO crystal or another HHG cell [34] will enable stabilized two- or three-color measurements. This scheme will preserve the metallic foils and also increase the lifetime of the mirrors.

Funding Information: ERC Starting Grant (contract 307270-ATTOSCOPE); NCCR-MUST, a funding instrument of the Swiss National Science Foundation; SNF (200021_159875).
T.G. and A.J. contributed equally to this work.

REFERENCES

1. A. McPherson, G. Gibson, H. Jara, U. Johann, T. S. Luk, I. A. McIntyre, K. Boyer, and C. K. Rhodes, J. Opt. Soc. Am. B **4**, 595 (1987).
2. M. Ferray, A. L'Huillier, X. F. Li, L. A. Lompre, G. Mainfray, and C. Manus, J. Phys. B: At. Mol. Opt. Phys. **21**, L31 (1988).
3. P. B. Corkum and F. Krausz, Nat. Phys. **3**, 381 (2007).
4. M. Drescher, M. Hentschel, R. Kienberger, M. Uiberacker, V. Yakovlev, a. Scrinzi, T. Westerwalbesloh, U. Kleineberg, U. Heinzmann, and F. Krausz, Nature. **419**, 803 (2002).
5. F. Calegari, D. Ayuso, A. Trabattoni, L. Belshaw, S. De Camillis, S. Anumula, F. Frassetto, L. Poletto, A. Palacios, P. Decleva, J. B. Greenwood, F. Martín, and M. Nisoli, Science. **346**, 336 (2014).
6. J. Wu, M. Magrakvelidze, L. Schmidt, M. Kunitski, T. Pfeifer, M. Schöffler, M. Pitzer, M. Richter, S. Voss, H. Sann, H. Kim, J. Lower, T. Jahnke, A. Czasch, U. Thumm, and R. Dörner, Nat. Commun. **4**, 2177 (2013).
7. H. Li, N. G. Kling, T. Gaumnitz, C. Burger, R. Siemering, J. Schötz, Q. Liu, L. Ban, Y. Pertot, J. Wu, A. M. Azzeer, R. de Vivie-Riedle, H. J. Wörner, and M. F. Kling, Opt. Express **25**, 14192 (2017).
8. M. Schultze, M. Fieß, N. Karpowicz, J. Gagnon, M. Korbman, M. Hofstetter, S. Neppl, A. L. Cavalieri, Y. Komninos, T. Mercouris, C. A. Nicolaides, R. Pazourek, S. Nagele, J. Feist, J. Burgdörfer, A. M. Azzeer, R. Ernstorfer, R. Kienberger, U. Kleineberg, E. Goulielmakis, F. Krausz, and V. S. Yakovlev, Science **328**, 1658 (2010).
9. M. Hentschel, R. Kienberger, C. Spielmann, G. A. Reider, N. Milosevic, T. Brabec, P. Corkum, U. Heinzmann, M. Drescher, and F. Krausz, Nature **414**, 509 (2001).
10. R. Kienberger, E. Goulielmakis, M. Uiberacker, A. Baltuska, V. Yakovlev, F. Bammer, A. Scrinzi, T. Westerwalbesloh, U. Kleineberg, U. Heinzmann, M. Drescher, and F. Krausz, Nature **427**, 817 (2004).
11. P. B. Corkum, Phys. Rev. Lett. **71**, 1994 (1993).
12. J. Seres, P. Wobrauschek, C. Streli, V. S. Yakovlev, E. Seres, F. Krausz, and C. Spielmann, New J. Phys. **8**, 251 (2006).
13. T. Popmintchev, M.-C. Chen, D. Popmintchev, P. Arpin, S. Brown, S. Alisauskas, G. Andriukaitis, T. Balciunas, O. D. Mucke, A. Pugzlys, A. Baltuska, B. Shim, S. E. Schrauth, A. Gaeta, C. Hernandez-Garcia, L. Plaja, A. Becker, A. Jaron-Becker, M. M. Murnane, and H. C. Kapteyn, Sci. (80-.). **336**, 1287 (2012).
14. T. Gaumnitz, A. Jain, Y. Pertot, M. Huppert, I. Jordan, F. Ardana-Lamas, and H. J. Wörner, Opt. Express **25**, 27506 (2017).
15. F. Krausz, Rev. Mod. Phys. **81**, 163 (2009).
16. A. von Conta, M. Huppert, and H. J. Wörner, Rev. Sci. Instruments **87**, 073102 (2016).
17. J. Itatani, J. Levesque, D. Zeidler, H. Niikura, H. Pépin, J. C. Kieffer, P. B. Corkum, and D. M. Villeneuve, Nature **432**, 867 (2004).
18. Q. Zhang, K. Zhao, J. Li, M. Chini, Y. Cheng, Y. Wu, E. Cunningham, and Z. Chang, Opt. Lett. **39**, 3670 (2014).
19. P. Rudawski, A. Harth, C. Guo, E. Lorek, M. Miranda, C. M. Heyl, E. W. Larsen, J. Ahrens, O. Prochnow, T. Binhammer, U. Morgner, J. Mauritsson, A. L'Huillier, and C. L. Arnold, The Eur. Phys. J. D **69**, 70 (2015).
20. N. Thiré, R. Maksimenka, B. Kiss, C. Ferchaud, P. Bizouard, E. Cormier, K. Osvay, and N. Forget, Opt. Express **25**, 1505 (2017).
21. S. Hädrich, M. Kienel, M. Müller, A. Klenke, J. Rothhardt, R. Klas, T. Gottschall, T. Eidam, A. Drozdy, P. Jójárt, Z. Várallyay, E. Cormier, K. Osvay, A. Tünnermann, and J. Limpert, Opt. Lett. **41**, 4332 (2016).
22. M. Müller, M. Kienel, A. Klenke, T. Gottschall, E. Shestaev, M. Plötner, J. Limpert, and A. Tünnermann, Opt. Lett. **41**, 3439 (2016).
23. J. Peatross, J. L. Chaloupka, and D. D. Meyerhofer, Opt. Lett. **19**, 942 (1994).
24. P. M. Paul, Science. **292**, 1689 (2001).
25. J. Miyazaki, K. Kawasumi, and T. Kobayashi, Opt. Lett. **39**, 4219 (2014).
26. D. Faccio, G. Tamošauskas, E. Rubino, J. Darginavičius, D. G. Papazoglou, S. Tzortzakis, A. Couairon, and A. Dubietis, Phys. Rev. E **86**, 036304 (2012).
27. V. N. Mahajan, J. Opt. Soc. Am. A **3**, 470 (1986).
28. A. Jain, T. Gaumnitz, and H. J. Wörner, publication **xxxx**, xxxx (2018).
29. I. Jordan, A. Jain, T. Gaumnitz, J. Ma, and H. J. Wörner, Rev. Sci. Instrum. **89** (2018).
30. T. Leitner, "High Order Harmonic Generation as a possible Seed Source for the BESSY Free Electron Laser," Ph.D. thesis, HU Berlin (2007).
31. M. Lewenstein, P. Balcou, and M. Ivanov, Phys. Rev. A **49** (1994).
32. M. V. Ammosov, N. B. Delone, and V. P. Krainov, Zh. Eksp. Teor. Fiz. **91**, 2008 (1986).
33. W. Boutu, S. Haessler, H. Merdji, P. Breger, G. Waters, M. Stankiewicz, L. J. Frasinski, R. Taieb, J. Caillat, A. Maquet, P. Monchicourt, B. Carre, and P. Salieres, Nat. Phys. **4**, 545 (2008).
34. V. Wanie, M. Galli, E. P. Månsson, M. C. Castrovilli, F. Légaré, F. Frassetto, L. Poletto, M. Nisoli, and F. Calegari, "Generation of Few-Cycle UV pulses Synchronized with Attosecond XUV Pulses," in "Conf. Lasers Electro-Optics," (OSA, Washington, D.C., 2018), p. JTu2A.158.